ACS APPLIED ENERGY MATERIALS

www.acsaem.org Article

Ultrastable Three-Dimensional Triptycene- and Tetraphenylethene-Conjugated Microporous Polymers for Energy Storage

Tzu-Hsin Weng, Mohamed Gamal Mohamed,* Santosh U Sharma, Swetha V Chaganti, Maha Mohamed Samy, Jyh-Tsung Lee, and Shiao-Wei Kuo*

Cite This: https://doi.org/10.1021/acsaem.2c02809 Read Online

ACCESS | Metrics & More | Article Recommendations | Supporting Information

ABSTRACT: In this study, we used one-pot polycondensation through Suzuki cross-coupling to prepare three three-dimensional (3D) conjugated microporous polymers (CMPs; Try-Ph-Th, Try-Ph-Py, and Try-Ph-TPE) containing triptycene (Try) moieties connected to thiophene (Th), pyrene (Py), and tetraphenylethene (TPE) units. Thermogravimetric analysis (TGA) revealed that the thermal stabilities of the Try-Ph-Py CMP (T_{d10} = 605 °C; char yield = 80 wt %) and the Try-Ph-TPE CMP (T_{d10} = 517 °C; char yield = 71 wt %) were higher than those of the Try-Ph-Th CMP (T_{d10} = 471 °C; char yield = 65 wt %) and other CMP materials. The Try-Ph-TPE CMP sample possessed a high specific surface area (up to 700 $m^2\ g^{-1}$) and pore volume (0.45 $cm^3\ g^{-1}$), based on N_2 adsorption/desorption analyses as well as superior electrochemical performance, characterized by a specific capacity of 245 F g^{-1} at a current density of 0.5 A g^{-1}. The Try-Ph-Th, Try-Ph-Py, and Try-Ph-TPE CMPs exhibited high-capacity retentions of 75.00, 85.71, and 92.85%, respectively. In addition to their extraordinary three-electrode performance, these CMPs provided high specific capacitances (53, 84.2, and 166 F g^{-1}, respectively) when used as real supercapacitors.

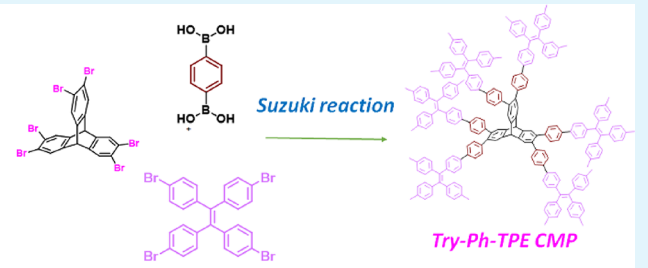

KEYWORDS: *Suzuki coupling, triptycene, tetraphenylethene, conjugated microporous polymers, supercapacitor*

INTRODUCTION

Increasing energy consumption and climate damage from the use of conventional fossil fuels are spurring the development of alternative energy sources and efficient energy storage devices. In particular, supercapacitors have become attractive devices because of their rapid charge/discharge switching, high power density, and long cycle life.[1−8] The storage of electrical charge in supercapacitors arises from their functioning as electrochemical pseudocapacitors or electrical double-layer capacitors (EDLCs).[9−13] Charge storage in pseudocapacitors, also known as redox supercapacitors, operates through reversible redox reactions occurring between the electrolyte and electrode materials.[14−17] In EDLCs, charge storage is more of a physical process, involving adsorption/desorption of charged ions at the interface between the electrolyte and the electrode; accordingly, EDLCs require a high surface area, a narrow and consistent pore size distribution, and a large pore volume if they are to provide high capacitance.[18,19] Porous organic polymers (POPs) are interesting materials because of their potential for application in various fields—especially for energy storage and gas capture.[20−36] According to IUPAC classification, porous materials can be divided into macroporous (pore diameter: >50 nm), mesoporous (2−50 nm), or microporous (<2 nm). POPs can also be defined in terms of their synthetic materials and their methods of constructed routes, for example, as covalent organic frameworks (COFs), covalent triazine frameworks (CTFs), hyper-crosslinked polymers (HCPs), and conjugated microporous polymers (CMPs).[37−46] CMPs are particularly interesting because they are amorphous materials possessing linked π-conjugated building blocks, where the sizes of the linkers can range from small phenyl units to bicyclic and macrocyclic moieties. These macromolecular networks have typically been constructed using such reactions as Sonogashira−Hagihara, Suzuki−Miyaura, and Yamamoto coupling. The large number of potential structural units and the many available synthetic methods allow optimization of the structures, skeletons, and properties of CMPs.[47−56] Triptycene (Try) has a paddle wheel shape, composed of three benzene units connected through two sp^3-hybridized carbon atoms, with D_{3h} symmetry; the three benzene rings are arranged relatively at angles of 120° with a huge volume of the surrounding aromatic skeleton.[57−63] Because of this characteristic structure, Try exhibits good thermal stability, mechanical properties, and porosity. In this

Received: August 30, 2022
Accepted: October 5, 2022

https://doi.org/10.1021/acsaem.2c02809
ACS Appl. Energy Mater. XXXX, XXX, XXX−XXX

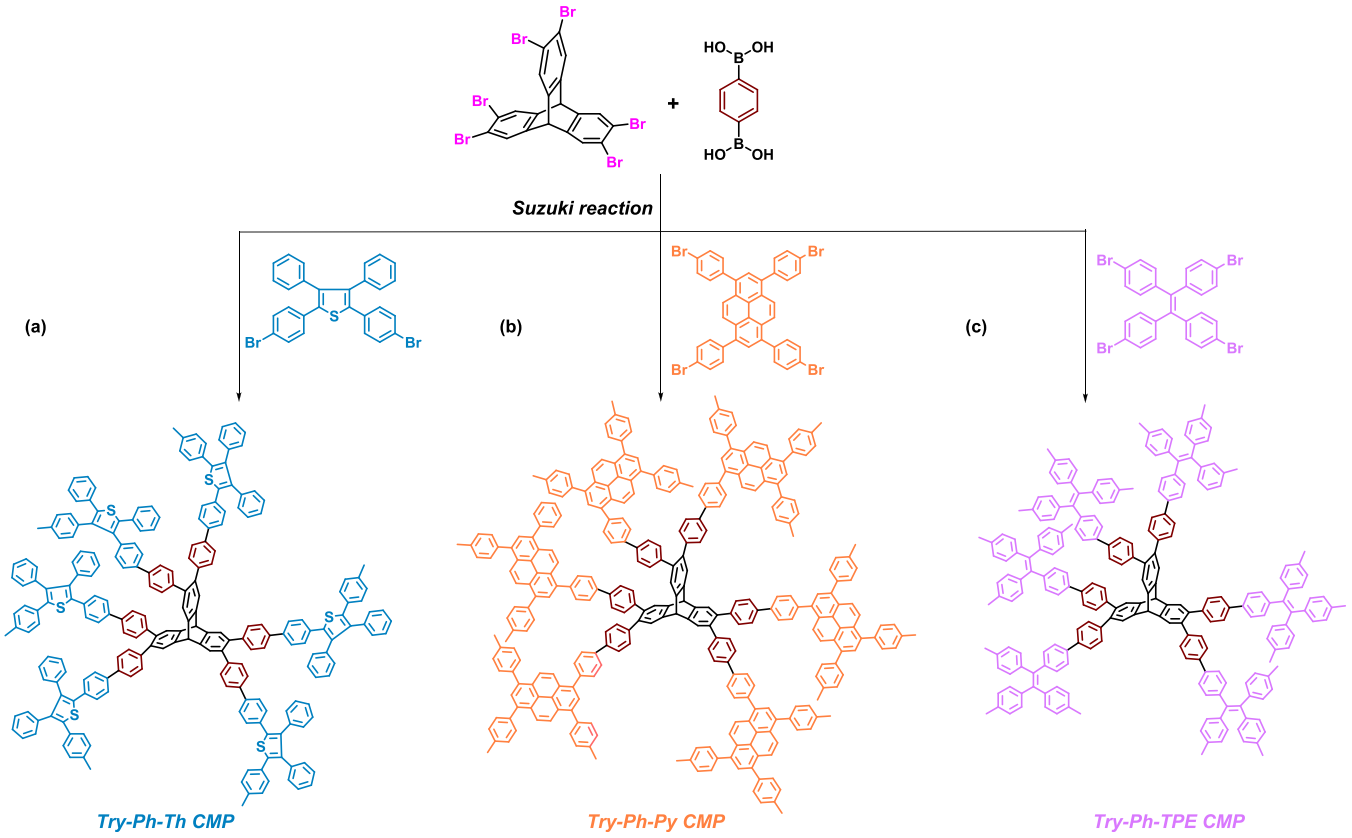

Figure 1. Schematic representation of the preparation of the (a) Try-Ph-Th, (b) Try-Ph-Py, and (c) Try-Ph-TPE CMPs.

study, we used a Try derivative as a building block to construct new CMP materials. Previously, Mastalerz et al. prepared metal-assisted salphen organic frameworks featuring three-dimensional (3D) Try moieties as a central monomer unit and applied them to gas adsorption.[60] Furthermore, the Nuckolls group constructed pseudocapacitors from porous materials containing 3D Try and perylene diimide units.[62] Recently, Das et al. employed a nitrogen- and oxygen-rich Try-based COF for the uptake of radioactive iodine.[61] Inspired by those previous reports, here, we inserted a 3D Try monomer into three CMPs (abbreviated Try-Ph-Th, Try-Ph-Py, and Try-Ph-TPE; Th, thiophene; Py, pyrene; TPE, tetraphenylethene) through one-pot polycondensations using Suzuki−Miyaura coupling. We then examined the chemical structures, morphologies, crystallinities, thermal degradation, char yields, and porosities of these 3D Try-CMPs. Because all of these 3D Try-CMPs possessed excellent thermal stabilities and high Brunauer−Emmett−Teller (BET) surface areas, we examined their potential utility in electrochemical applications. Interestingly, measurements of three-electrode systems and symmetric supercapacitor coin cells containing these porous 3D Try-CMPs revealed their suitability for real and hybrid electrical energy storage applications.

EXPERIMENTAL SECTION

Materials. Benzophenone (99%), bromine (Br_2), sodium thiosulfate, thiophene (Th), zinc (Zn, 98%), titanium tetrachloride ($TiCl_4$, 99.9%), benzene diboronic acid (Ph-2BO, 98%), benzeneboronic acid [$PhB(OH)_2$], 1,4-dioxane (DO), potassium carbonate (K_2CO_3, 99.9%), Try, anhydrous magnesium sulfate ($MgSO_4$, 99.5%), tetrahydrofuran (THF), acetone, ethanol (EtOH), dichloromethane (DCM), dimethylformamide (DMF), methanol (MeOH), and chloroform ($CHCl_3$) were purchased from Alfa Aesar. $Pd(PPh_3)_4$ was obtained from Sigma-Aldrich. 1,3,6,8-Tetrakis(4-bromophenyl)pyrene (Py-Ph-Br_4) and tetraphenylethene (TPE) were synthesized according to Schemes S1 and S2, respectively.[46] Py-Ph-Br_4 had T_{d10} = 281 °C and char yield = 48 wt % (by thermogravimetric analysis (TGA); Figure S1).

Synthesis of Tetraphenylethylene (TPE). Under N_2, a mixture of Zn (4.31 g, 65.9 mmol) and benzophenone (3.00 g, 16.4 mmol) in THF (100 mL) was stirred at 0 °C for 10 min. After adding $TiCl_4$ (3.60 mL, 33.0 mmol), the mixture was warmed to 80 °C for 24 h. Finally, add 5% aqueous K_2CO_3 into the reaction mixture. Then, THF was removed under reduced pressure, and the remaining solution was extracted three times with EtOAc, and then to remove EtOAc, it was dried over $MgSO_4$ and removed to obtain TPE as a white solid (Scheme S2; 2.66 g, 97%, mp = 229 °C by differential scanning calorimetry (DSC); Figure S2). FTIR (KBr, cm^{-1}; Figure S3): 3047 (aromatic C−H stretching), 1602 (C═C stretching). ^1H NMR (500 MHz, $CDCl_3$, δ, ppm; Figure S4): 7.08−7.09 (12H), 7.01−7.03 (6H). ^{13}C NMR (125 MHz, $CDCl_3$, δ, ppm; Figure S5): 140.70−126.4.

1,1,2,2-Tetrakis(4-bromophenyl)ethene (TPE-Br_4). Br_2 (4.00 mL, 80.0 mmol) was added to a mixture of TPE (3.32 g, 10.0 mmol), DCM (20 mL), and glacial acetic acid (10 mL) in a reaction flask at 0 °C (ice bath). The mixture solution was stirred at room temperature for 48 h, and then it was extracted three times with water. The resulting white powder was recrystallized using a mixture of DMC/MeOH to obtain pure TPE-Br_4 (Scheme S3; 6.15 g, 95%). mp = 261−262 °C [DSC; Figure S6]. FTIR (KBr, cm^{-1}): 3051 (aromatic C−H stretching), 1572 (C═C stretching). ^1H NMR (500 MHz, $CDCl_3$, δ, ppm; Figure S7): 7.27 (8H), 6.86 (18H). ^{13}C NMR (125 MHz, $CDCl_3$, δ, ppm; Figure S8): 142.30−121.80. T_{d10} = 354 °C; char yield = 0.7 wt % (by TGA; Figure S9).

2,3,4,5-Tetrabromothiophene (Th-Br_4). Br_2 (5.3 mL, 0.033 mmol) and Th (2.0 g, 0.023 mmol) were dissolved in $CHCl_3$ (30 mL) at 0 °C, and then the mixture was heated under reflux for 24 h. After cooling, the solution was added to cool saturated sodium thiosulfate. The obtained solid was collected and washed with hot EtOH to provide Th-Br_4 as a white powder (Scheme S4; 80%; T_m = 119 °C). FTIR (KBr,

https://doi.org/10.1021/acsaem.2c02809
ACS Appl. Energy Mater. XXXX, XXX, XXX−XXX

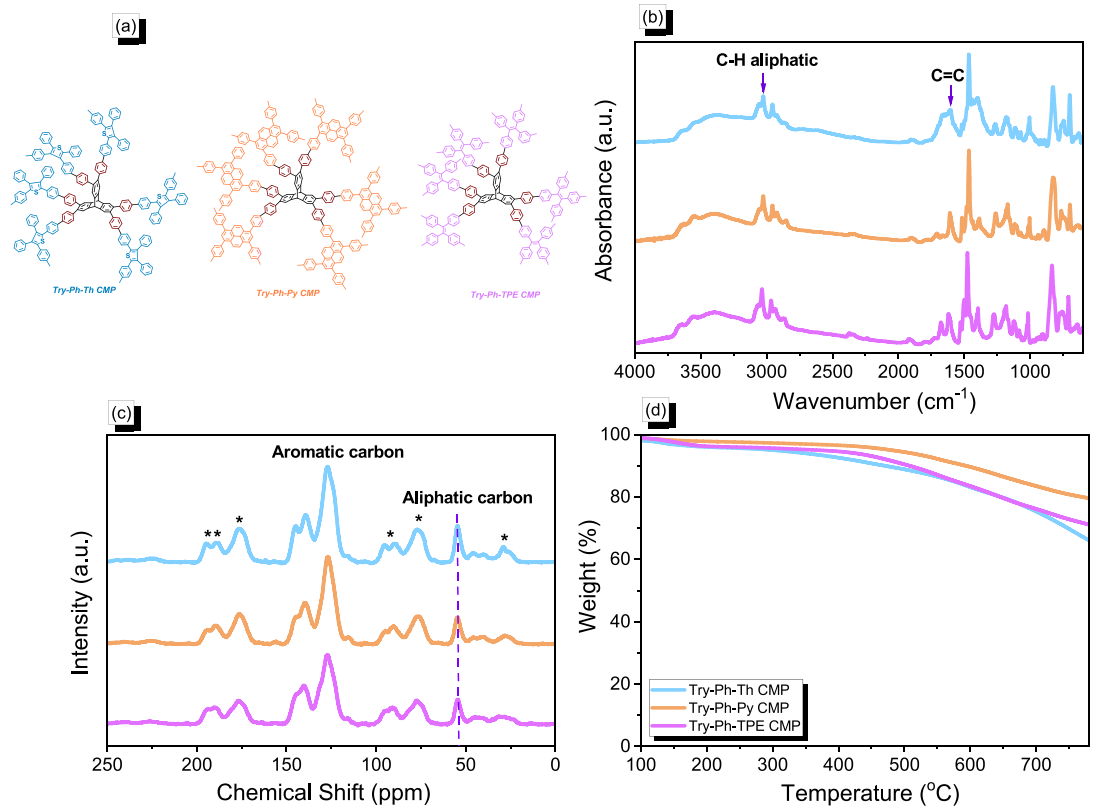

Figure 2. (a) Chemical structures, (b) FTIR spectra, (c) solid-state NMR spectra, and (d) TGA traces of the Try-Ph-Th, Try-Ph-Py, and Try-Ph-TPE CMPs.

cm^{-1}): 1636 (C═C), 852 (C−S). ^1H NMR (500 MHz, DMSO-d_6, δ, ppm; Figure S10): no peaks detected. ^{13}C NMR (125 MHz, $CDCl_3$, δ, ppm; Figure S11): 116.936, 110.284.

2,3,4,5-Tetraphenylthiophene (Th-4Ph). A mixture of Th-Br_4 (2.00 g, 1.40 mmol), $Pd(PPh_3)_4$ (0.30 g, 0.050 mmol), $PhB(OH)_2$ (3.70 g, 6.53 mmol), and K_2CO_3 (8.30 g, 16.6 mmol) was degassed three times under N_2. DO (50 mL) and H_2O (10 mL) were added, and then the mixture was heated at 90 °C for 48 h. The solution was placed in ice-cold H_2O and neutralized with HCl (2 mL). The powder was filtered off, washed with water and MeOH, and dried to produce a white powder (Scheme S4). FTIR (KBr, cm^{-1}; Figure S12): 3063 (C−H aromatic), 1595 (C═C), 1493, 1456, 1075, 1028, 912. ^1H NMR (500 MHz, DMSO-d_6, δ, ppm; Figure S13): 7.25 (4H), 7.12 (8H), 6.97 (8H). ^{13}C NMR (125 MHz, DMSO-d_6, δ, ppm; Figure S14): 140.31−127.74.

2,5-Bis(4-bromophenyl)-3,4-diphenylyhiophene (Th-Ph-Br_2). A solution of Th-4Ph (5.00 g, 12.8 mmol) and Br_2 (4.20 g, 26.28 mmol) in $CHCl_3$ (40 mL) was stirred at 0 °C (ice bath) for 4 h. After evaporation of the solvent, the residue was washed with EtOH to give a yellow solid (Scheme S5, 85%). FTIR (KBr, cm^{-1}): 3047.38 (C−H aromatic), 1491.15, 1437.03, 1074.84. ^1H NMR (500 MHz, DMSO-d_6, δ, ppm; Figure S15): 7.37, 7.15, 7.08, 6.95, 6.79 (CH aromatic). ^{13}C NMR (125 MHz, DMSO-d_6, δ, ppm; Figure S16): 140.87−121.97 (Th and aromatic carbon nuclei). T_{d10} = 331 °C and char yield = 0.3 wt % (by TGA; Figure S17).

2,3,6,7,14,15-Hexabromotriptycene (Try-Br_6). A mixture of Try (1.00 g, 3.90 mmol), Fe (0.080 g, 1.4 mmol), I_2 (0.13 g, 0.40 mmol), and Br_2 (1.49 mL, 39.0 mmol) in $CHCl_3$ (80 mL) was stirred in a round-bottom flask at 65 °C for 24 h. The excess Br_2 and $CHCl_3$ were evaporated under reduced pressure. The obtained solid was washed with EtOH for 2 h. Column chromatography (eluent: hexane) provided Try-Br_6 as a solid (Scheme S6; 75%; T_m > 350 °C). FTIR (KBr, cm^{-1}): 3060 (C−H aromatic), 2924 (C−H aliphatic), 1446, 1355, 1095, 930.70, 881.69. ^1H NMR (500 MHz, DMSO-d_6, δ, ppm; Figure S18): 7.61 (CH aromatic), 5.81 (CH aliphatic). ^{13}C NMR (125 MHz, DMSO-d_6, δ, ppm; Figure S19): 144.37, 129.54, 122.99, 51.30 (aliphatic carbon nuclei). T_{d10} = 461 °C and char yield = 4 wt % (by TGA; Figure S20).

Try-Ph-Th, Try-Ph-Py, and Try-Ph-TPE CMPs. A solution of Try-Br_6 (0.20 g, 0.27 mmol), Ph-2BO (0.14 g, 0.84 mmol), Th-Ph-Br_2 (0.070 g, 0.13 mmol) [or Py-Ph-Br_4 (0.070 g, 0.085 mmol) or TPE-Br_4 (0.060 g, 0.092 mmol)], K_2CO_3 (0.38 g, 10 mmol), and $Pd(PPh_3)_4$ (0.10 g, 0.10 mmol) in DMF (8 mL) and H_2O (2 mL) was degassed three times under vacuum and then stirred at 80 °C for 72 h. The gray solid was filtered off and washed several times with H_2O, THF, MeOH, and acetone. The gray powder of Try-Ph-Th, green solid of Try-Ph-Py, and green powder of Try-Ph-TPE CMPs were dried at 100 °C; their syntheses are displayed in Figure 1a−c, respectively. Elemental analysis for Try-Ph-Th CMP: C, 81.71%; H, 5.11%; S, 6.18. Elemental analysis for Try-Ph-Py CMP: C, 86.71%; H, 4.52%. Elemental analysis for Try-Ph-TPE CMP: C, 88.26%; H, 4.10%.

RESULTS AND DISCUSSION

Synthesis and Characterization of 3D CMPs Containing Try Units. Th-Ph-Br_2 was prepared in three steps, as displayed in Schemes S4 and S5. First, Th-Br_4 was synthesized through the reaction of Th with Br_2 in $CHCl_3$ under reflux. Next, Th-4Ph was prepared in high yield through Suzuki coupling of Th-Br_4 with $PhB(OH)_2$ in toluene in the presence of K_2CO_3 and $Pd(PPh_3)_4$. Finally, the bromination of Th-4Ph with Br_2 in DCM afforded Th-Ph-Br_2 as a yellow solid. Try-Br_6 was prepared as a white solid in good yield through the reaction of Try with Br_2 in $CHCl_3$ in the presence of small amounts of Fe and I_2 (Scheme S6). Nuclear magnetic resonance (NMR) and Fourier transform infrared (FTIR) spectra confirmed the successful synthesis of Th-Ph-Br_2, Py-Ph-Br_4, TPE-Br_4, and Try-Br_6 [see the Experimental Section and Supporting Information (SI)].

https://doi.org/10.1021/acsaem.2c02809
ACS Appl. Energy Mater. XXXX, XXX, XXX−XXX

Table 1. TGA, BET, and Capacitance Data of the 3D Try-CMPs

sample	T_{d10} (°C)	char yield (wt %)	surface area ($m^2\ g^{-1}$)	pore volume ($cm^3\ g^{-1}$)	pore size (nm)	capacity at 0.5 A g^{-1} ($F\ g^{-1}$)
Try-Ph-Th CMP	471	65	364	0.25	1.75	114
Try-Ph-Py CMP	605	80	611	0.36	1.51	152
Try-Ph-TPE CMP	517	71	715	0.45	1.06−1.68	245

Figure 1 displays the synthetic routes we used to prepare our three 3D CMPs through efficient Suzuki polymerizations in mixtures of DMF and H_2O with K_2CO_3 as the base and Pd as the catalyst. The Try-Ph-Th CMP was obtained as gray powder from the reaction of Try-Br_6 with Th-Ph-Br_2 and Ph-2BO [Figure 1a]; the Try-Ph-Py CMP was obtained as a green solid from the reaction of Try-Br_6 with Py-Ph-Br_4 and Ph-2BO [Figure 1b]; and the Try-Ph-TPE CMP was obtained as a green solid from the reaction of Try-Br_6 with TPE-Br_4 and Ph-2BO [Figure 1c]. The three isolated 3D CMPs containing Try units were insoluble in all tested solvents, including MeOH, H_2O, DMF, DMSO, DCM, $CHCl_3$, THF, and acetone, suggesting that they possessed high crosslinking densities and high degrees of polymerization, thereby implying high degrees of porosity and high specific surface areas.

We used FTIR spectroscopy, solid-state ^{13}C NMR spectroscopy, and TGA to examine the chemical structures and thermal stabilities of the Try-Ph-Th, Try-Ph-Py, and Try-Ph-TPE CMPs (Figure 2). The FTIR spectrum [Figure S21a] of Try-Br_6 displayed the absorption band centered at 3060 and 2924 cm^{-1} for the C−H aromatic and C−H aliphatic units. The FTIR spectra [Figures S21b, S22b, and S23b] of Th-Ph-Br_2, Py-Ph-Br_4, and TPE-Br_4 showed the absorption peaks in the range of 3051−3047 cm^{-1} due to the presence of phenyl rings in their chemical structures. The FTIR spectra of all three CMPs featured their main characteristic absorption peaks in the ranges of 3038−3026, 2969−2958, and 1620−1598 cm^{-1}, representing the stretching vibrations of their C−H aromatic, C−H aliphatic (Tyr unit), and C═C bonds, respectively [Figure 2b and Figures S21c, S22c, and S23c]. In the solid-state NMR spectra, the signals of the aromatic carbon nuclei of the Try-Ph-Th, Try-Ph-Py, and Try-Ph-TPE CMPs appeared in the ranges of 146.00−116.60, 145.22−115.15, and 144.80−116.41 ppm,

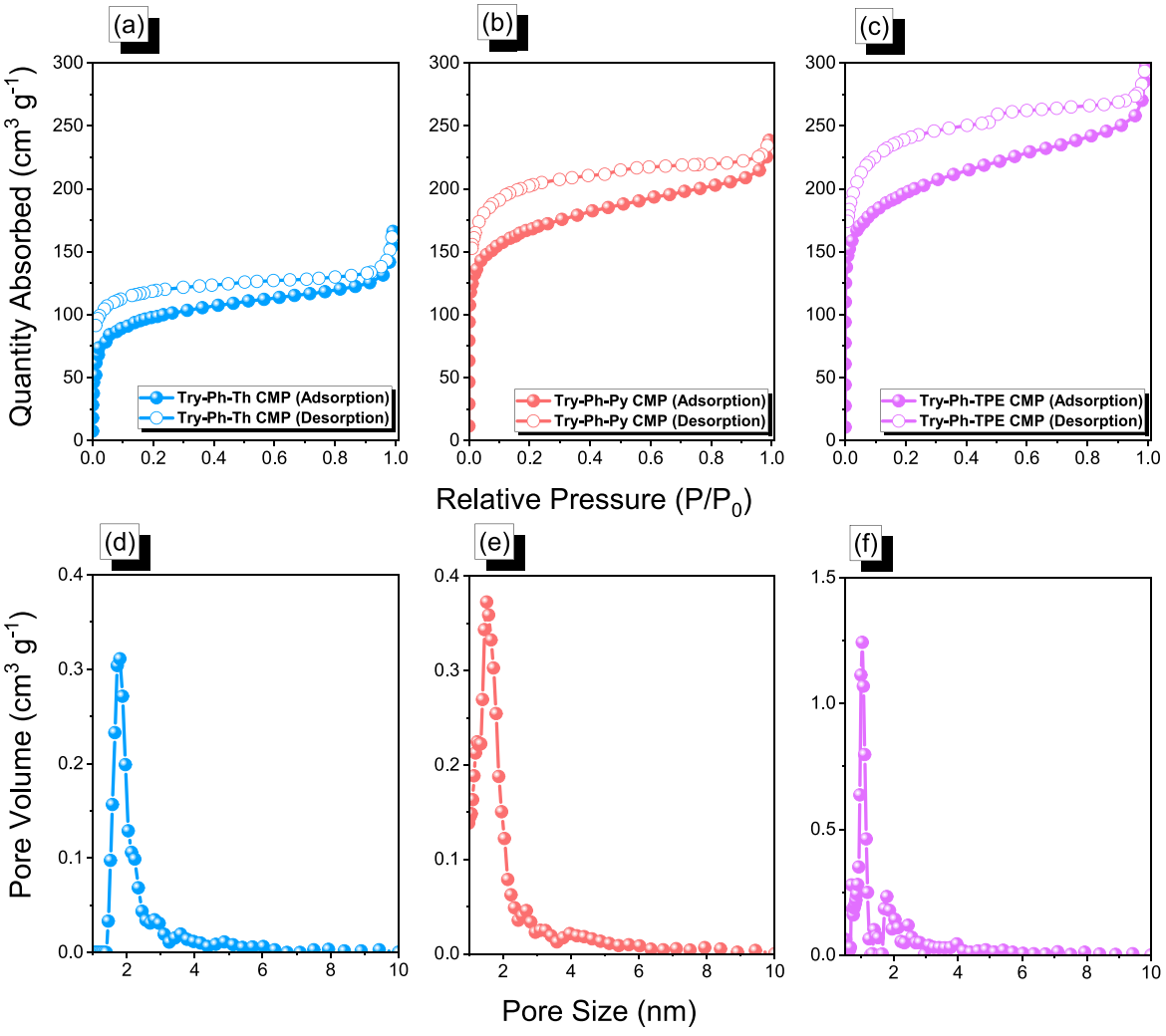

Figure 3. (a−c) N_2 adsorption/desorption isotherms and (d−f) pore size distribution patterns of the (a and d) Try-Ph-Th, (b and e) Try-Ph-Py, and (c and f) Try-Ph-TPE CMPs.

https://doi.org/10.1021/acsaem.2c02809
ACS Appl. Energy Mater. XXXX, XXX, XXX−XXX

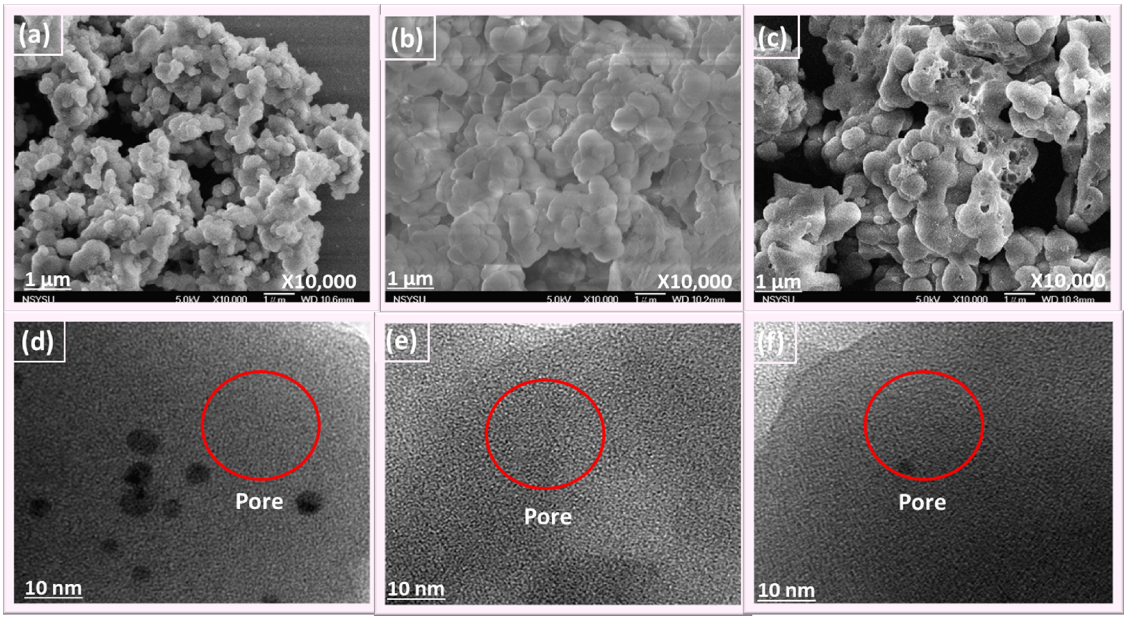

Figure 4. (a–c) SEM and (d–f) TEM images of the (a and d) Try-Ph-Th, (b and e) Try-Ph-Py, and (c and f) Try-Ph-TPE CMPs.

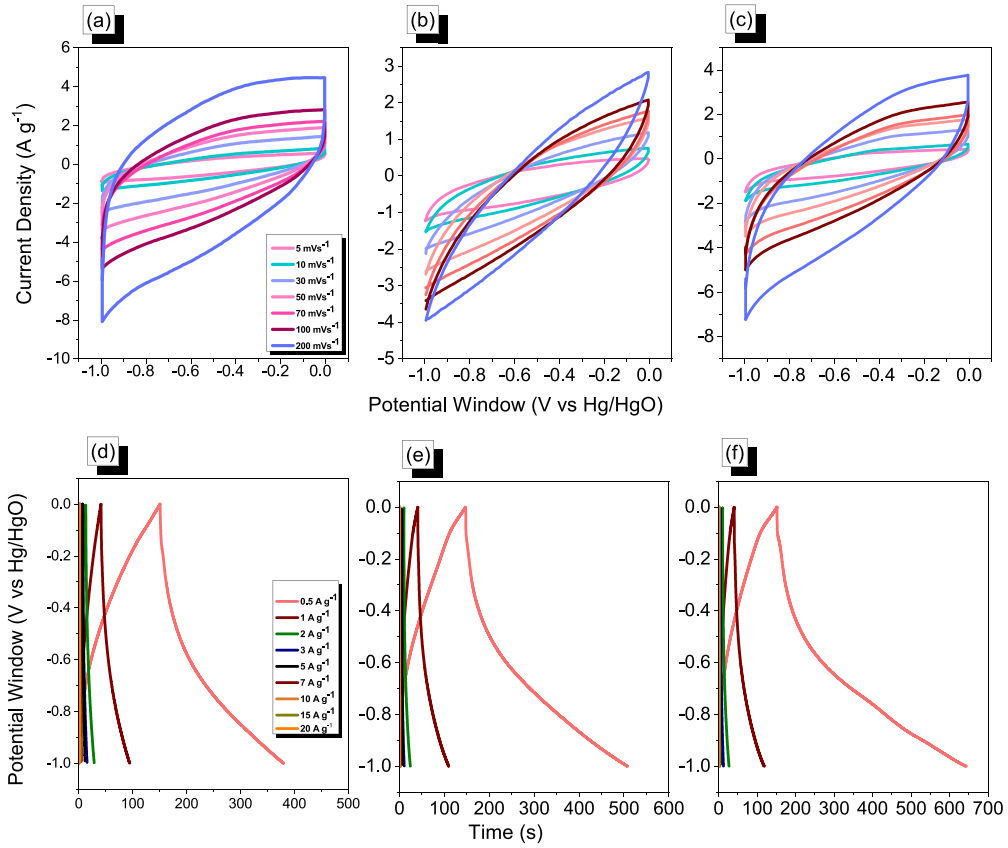

Figure 5. (a–c) CV and (d–f) GCD curves of the (a and d) Try-Ph-Th, (b and e) Try-Ph-Py, and (c and f) Try-Ph-TPE CMPs. From their GCD curves, we estimated the specific capacitances of the Try-Ph-Th, Try-Ph-Py, and Try-Ph-TPE CMPs at 0.5 A g^{-1} to be 114, 152, and 245 F g^{-1}, respectively. Furthermore, at current densities of 0.5, 1, 2, 3, 6, 7, 10, 16, and 20 A g^{-1}, the specific capacitances [Figure 6a] for the Try-Ph-Th CMP were 114, 53, 31, 25, 20, 18, 16, 14, and 13 F g^{-1}, respectively; for the Try-Ph-Py CMP, they were 152, 60, 26, 14, 14, 7, 4, 3, and 2 F g^{-1}, respectively; and for the Try-Ph-TPE CMP, they were 245, 78, 34, 24, 15, 12, 9, 7, and 6 F g^{-1}, respectively. Thus, among our three as-prepared CMPs used as electrode materials, the Try-Ph-TPE CMP (245 F g^{-1}) delivered the highest specific capacitance, followed by the Try-Ph-Py (152 F g^{-1}) and Try-Ph-Th (114 F g^{-1}) CMPs. Based on their BET surface areas, we had expected the Try-Ph-TPE CMP to deliver the highest capacity.

respectively [Figure 2c]. Signals at 54.22, 54.69, and 54.69 ppm confirmed the successful incorporation of Try moieties in the frameworks of the Try-Ph-Th, Try-Ph-Py, and Try-Ph-TPE CMPs, respectively [Figure 2c]. We performed TGA by heating

https://doi.org/10.1021/acsaem.2c02809
ACS Appl. Energy Mater. XXXX, XXX, XXX−XXX

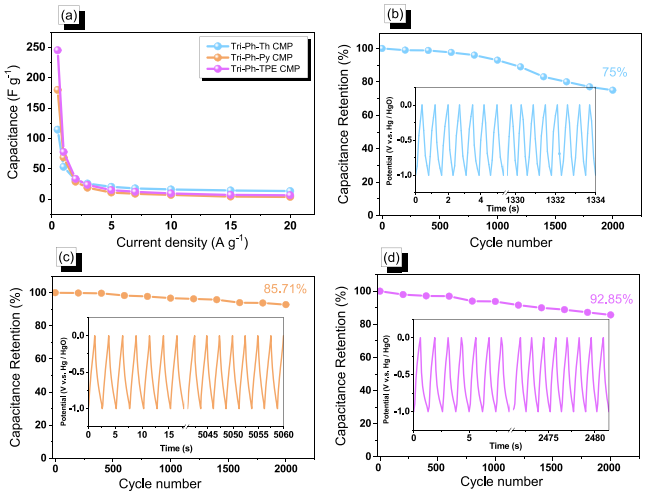

Figure 6. (a) Capacitance performance and (b−d) capacitance retention of the (b) Try-Ph-Th, (c) Try-Ph-Py, and (d) Try-Ph-TPE CMPs.

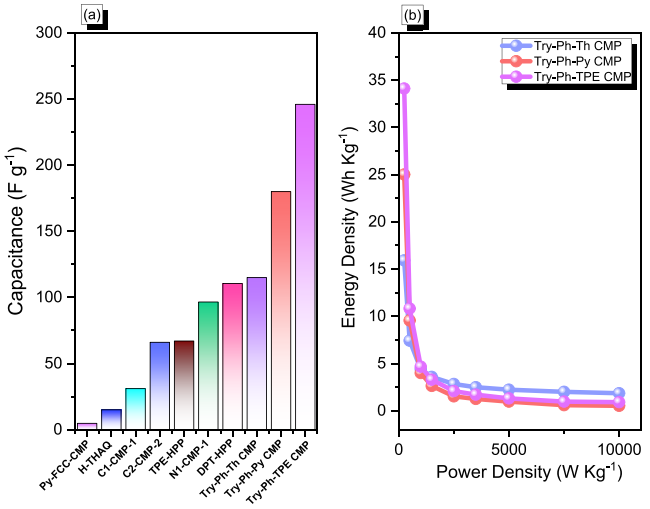

Figure 7. (a) Performance data of 3D Try-CMP precursors as organic electrodes compared with those of other CMPs. (b) Ragone plots of the 3D Try-CMP precursors.

Table 2. Characteristics of Fitted Nyquist Plots of the 3D Try-CMPs

sample	R_s (Ω)	R_{ct} (Ω)	CPE-EDL (S·s^n)	CPE-P (S·s^n)
Try-Ph-Th CMP	62.03	4000	6.91×10^{-5}	2.01×10^{-4}
Try-Ph-Py CMP	39.66	443.1	1.91×10^{-4}	1.25×10^{-3}
Try-Ph-TPE CMP	23.16	205.1	7.15×10^{-5}	6.80×10^{-4}

all three CMPs from 40 to 800 °C under N_2 atmospheres [Figure 2d and Table 1]. The 10% weight losses of the Try-Ph-Th, Try-Ph-Py, and Try-Ph-TPE CMPs under N_2 occurred at temperatures of 471, 605, and 517 °C, respectively. The char yields at 800 °C for the Try-Ph-Th, Try-Ph-Py, and Try-Ph-TPE CMPs were 65, 80, and 71 wt %, respectively. The TGA data suggested that all Try-CMP materials were the most stable thermal stability compared with their corresponding monomers according to TGA analyses. Nevertheless, all three of these 3D CMPs based on Try units exhibited excellent thermal stabilities at temperatures as high as 800 °C, making them potentially suitable for use in many real applications.

We performed N_2 adsorption/desorption measurements at 77 K to examine the porosities of the three Try-CMPs (Figure 3 and Table 1). The N_2 adsorption profiles [Figure 3a−c] of all three 3D Try-CMPs revealed sharp degrees of N_2 capture at values of P/P_0 of less than 0.01 and rapid increases in N_2 capture for values greater than 0.9. The presence of clear hysteresis during the desorption processes of the Try-Ph-Py and Try-Ph-TPE CMPs indicated that their framework structures featured both mesoporous and microporous characteristics.[20,46] In addition, the N_2 isotherm profiles of the Try-Ph-Th, Try-Ph-Py, and Try-Ph-TPE CMPs were type I and type IV curves (according to IUPAC classification), indicative of hierarchical porous structures. The BET surface areas and total pore volumes were 364 $m^2\ g^{-1}$ and 0.25 $cm^3\ g^{-1}$, respectively, for the Try-Ph-Th CMP; 611 $m^2\ g^{-1}$ and 0.36 $cm^3\ g^{-1}$, respectively, for the Try-Ph-Py CMP; and 715 $m^2\ g^{-1}$ and 0.45 $cm^3\ g^{-1}$, respectively, for the Try-Ph-TPE CMP. Applying nonlocal density functional theory (NLDFT), we determined the pore diameters of the Try-Ph-Th, Try-Ph-Py, and Try-Ph-TPE CMPs to be 1.75, 1.51, and 1.06−1.68 nm, respectively [Figure 3d−f]. The nanoscale dimensions of these pores implied the presence of meso- and microporosity in these Try-CMP frameworks. Furthermore, powder X-ray diffraction (PXRD) revealed the amorphous characteristics of these three Try-CMPs [Figure S24a−c].

We also used field emission scanning electron microscopy (FE-SEM) and high-resolution transmission electron microscopy (HR-TEM) to examine the morphologies of the porous Try-Ph-Th, Try-Ph-Py, and Try-Ph-TPE CMPs (Figure 4). All three Try-CMPs contained small agglomerated spherical particles, according to FE-SEM imaging [Figure 4a−c]. The HR-TEM images [Figure 4d−f] indicated the presence of bright and alternating dark regions, probably indicating that all of the Try-CMPs featured porous networks. The compositions and various elements in the chemical structures of the Try-Ph-Th, Try-Ph-Py, and Try-Ph-TPE CMPs [Figure 2a] were confirmed using SEM-EDS (energy-dispersive X-ray scattering) and TEM-EDX (energy-dispersive X-ray spectroscopy). Evidence for the existence of carbon and sulfur atoms distributed homogeneously in the Try-Ph-Th CMP framework, and for carbon atoms in the Try-Ph-Py and Try-Ph-TPE CMP skeletons, is provided in Figures S25−S28. Also, the X-ray photoelectron spectra (XPS) confirmed the presence of C and S elements in the Try-Ph-Th CMP and C element in both Try-Ph-Py and Try-Ph-TPE CMPs [Figure S29].

Electrochemical Analysis and Electrochemical Impedance Spectra of the 3D Try-CMPs. Many CMP compounds have already proven to be reliable electrode materials for various forms of energy storage devices[45,48] because of their extraordinarily high surface areas, redox-active moieties, and stable chemical morphologies during application. In this study, we evaluated the electrochemical performance of the Try-Ph-Th, Try-Ph-Py, and Try-Ph-TPE CMPs through cyclic voltammetry (CV) and galvanostatic charge/discharge (GCD) curves within the potential range from −1.0 to 0.0 V, with 1.0 M aqueous KOH as the electrolyte. Figure 5a−c displays the CV traces of the Try-Ph-Th, Try-Ph-Py, and Try-Ph-TPE CMPs recorded at scan rates between 5 and 200 mV s^{-1}. For each compound, the curves were rectangular, suggesting the combined effects of EDLC and pseudocapacitance. The CV curves persisted at higher scan rates; because current density increases with respect to the sweeping rate, these materials displayed high stability, rate capability, and kinetics. Figure 5d,e presents the GCD curves of the Try-Ph-Th, Try-Ph-Py, and Try-

https://doi.org/10.1021/acsaem.2c02809
ACS Appl. Energy Mater. XXXX, XXX, XXX−XXX

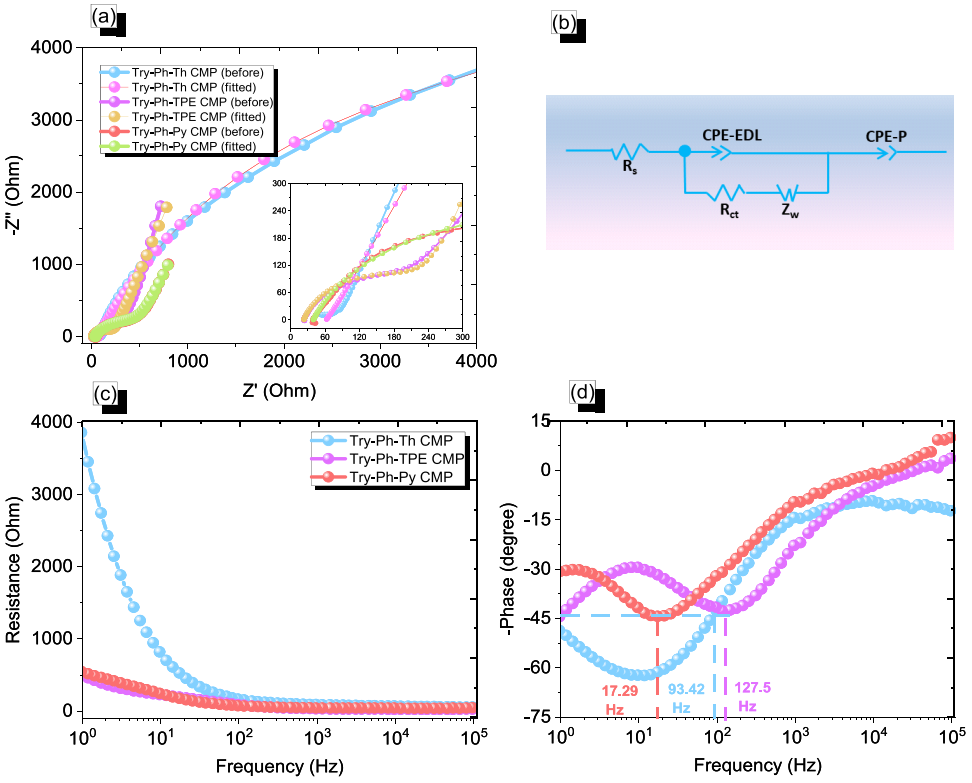

Figure 8. (a) Nyquist plots, (b) equivalent fitted circuit, (c) Bode plots of frequency-dependent resistance (magnitude), and (d) Bode plots of frequency-dependent phase angles for the Try-Ph-Th, Try-Ph-Py, and Try-Ph-TPE CMPs.

Ph-TPE CMPs recorded at current densities in the range of 0.5−20 A g^{-1}. The GCD curves of these CMPs were triangular with slight bends, indicating the presence of both EDLC and pseudocapacitive behavior. In addition, the discharging times of all of the CMPs were longer than the charging times, suggesting that these materials possessed high capacities.

We also evaluated the long-term cycling stabilities of these electrode materials [Figure 6a−c] over 2000 charge/discharge cycles at a relatively high current density of 10 A g^{-1}. The capacity retentions for the Try-Ph-Th, Try-Ph-Py, and Try-Ph-TPE CMPs were 75.00, 85.71, and 92.85%, respectively. Thus, among these three porous compounds, the Try-Ph-TPE CMP delivered the most outstanding capacity retention of greater than 92% after long-term cycling. The extraordinary behavior of this Try-Ph-TPE CMP can be explained by considering its high BET surface area. The electrochemical performance of our three Try-CMP materials was excellent when compared with that of other porous materials [Figure 7a and Table S1].[7,36,42] The Ragone plots in Figure 7b reveal that the energy densities of the Try-Ph-Th, Try-Ph-Py, and Try-Ph-TPE CMPs in three-electrode systems were 16, 25, and 34.1 W h kg^{-1}, respectively.

Electrochemical impedance spectroscopy (EIS) can be an excellent tool for characterizing electrode−electrolyte interfaces in a specific frequency domain. It provides information about the internal resistances offered by the electrode material and the electrolyte system. Here, we recorded the EIS spectra of our CMPs, using an aqueous solution of 1.0 M KOH as the electrolyte. We fitted the obtained EIS curves to an equivalent circuit containing an equivalent series resistance (R_s), a charge transfer resistance (R_{ct}), constant phase elements representing EDLC (CPE-EDL) and pseudocapacitive (CPE-P) behavior, and a Warburg element (Zw). Table 2 lists the obtained fitted data.

According to this data, Figure 8a,b presents the Nyquist plots and electrical equivalent circuits, respectively, of the Try-Ph-Th, Try-Ph-Py, and Try-Ph-TPE CMPs. The values of the initial series resistance, also known as the ohmic resistance, offered by the Try-Ph-Th, Try-Ph-Py, and Try-Ph-TPE CMPs were 62.03, 39.66, and 23.16 Ω, respectively. Thus, among these three three-electrode materials, the Try-Ph-TPE CMP displayed the lowest resistance and, hence, delivered the highest specific capacitance. Figure 8c displays the frequency-dependent magnitude Bode plots, revealing lines with negative slope in the low-frequency region, along with modest resistance in the higher-frequency region. From this information, we predicted extraordinary capacitive behavior for all three of these porous materials when used as electrode materials for energy application.[64−67]

Figure 8d presents the frequency-dependent phase-angle Bode plots for all three electrodes, revealing the calculated knee frequencies. The knee frequency is a measure of the rate performance of an electrode material, usually obtained when the phase angle becomes 45°. Under such conditions, both the capacitive and resistive properties become equal. The knee frequencies for the Try-Ph-Th, Try-Ph-Py, and Try-Ph-TPE CMPs were 93.42, 17.29, and 127.5 Hz, respectively. Thus, the knee frequency of the Try-Ph-TPE CMP was higher than those of the other electrodes, suggesting its extraordinary performance when employed as an electrode material in energy storage applications.[64−67]

Electrochemical Characteristics of Symmetrical Supercapacitor Coin Cells Incorporating the 3D Try-CMPs. Our evaluation of the practical use of these porous compounds included building symmetrical supercapacitor coin cells as well as examining their three-electrode performance. To build the coin cells, we adopted the CR2032 structure, consisting of bottom and top covers, a metal spring, a separator,

https://doi.org/10.1021/acsaem.2c02809
ACS Appl. Energy Mater. XXXX, XXX, XXX−XXX

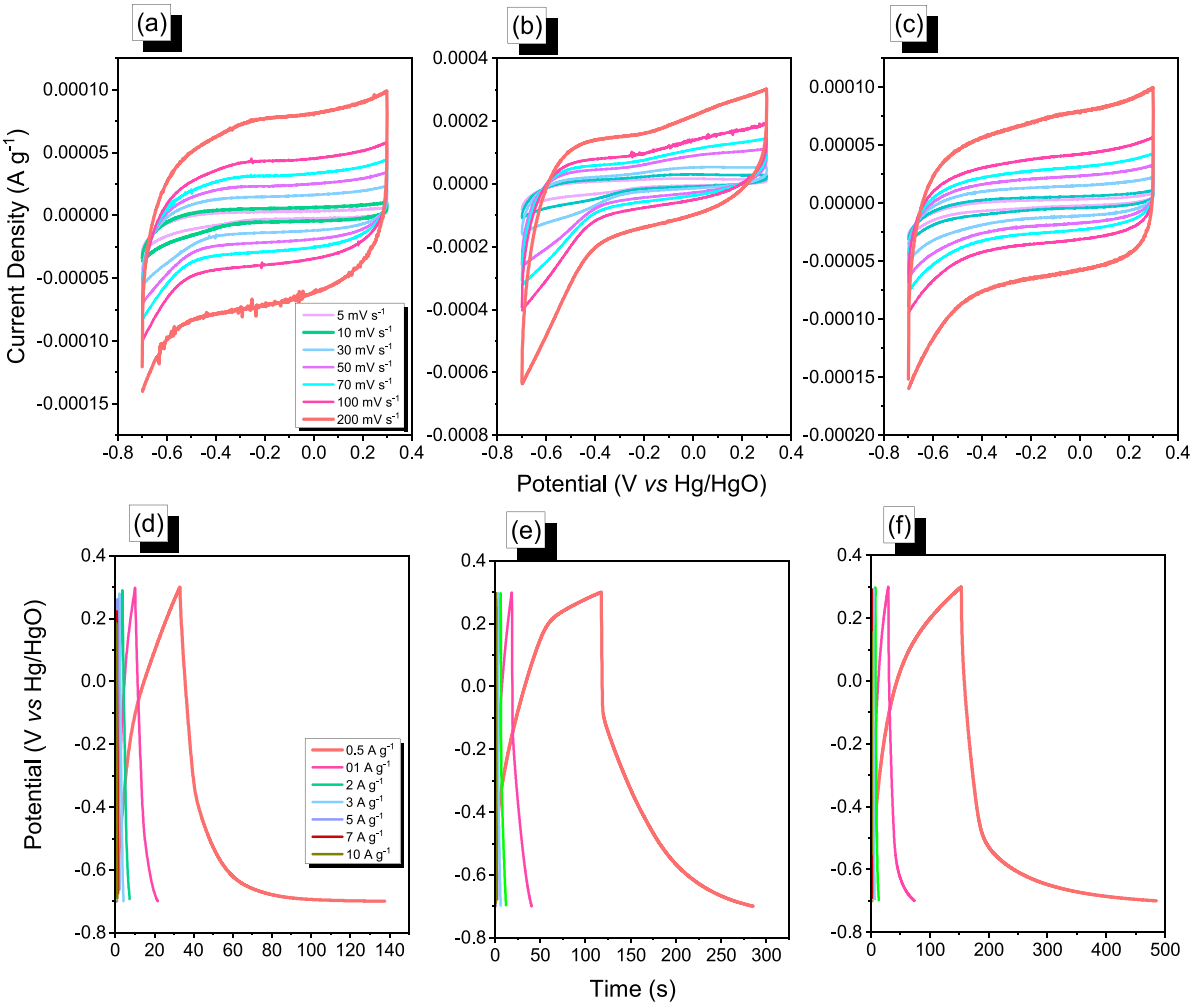

Figure 9. (a–c) CV and (d–f) GCD curves of symmetrical supercapacitor coin cells incorporating the (a and d) Try-Ph-Th, (b and e) Try-Ph-Py, and (c and f) Try-Ph-TPE CMPs.

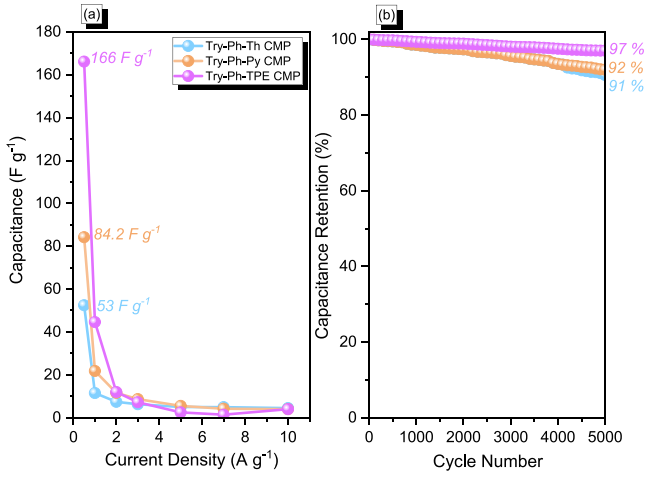

Figure 10. (a) Specific capacitance and (b) stability of symmetrical supercapacitor coin cells incorporating the Try-Ph-Th, Try-Ph-Py, and Try-Ph-TPE CMPs.

an anode and a cathode, and an electrolyte. To build symmetrical supercapacitors, we used our CMPs as both the cathode and the anode. A slurry, made in accordance with our previous report,[30] was cast onto carbon paper. We employed a Selemion AMV membrane with aqueous 1.0 M KOH as the electrolyte. All electrochemical measurements were performed at potentials between −0.7 and +0.3 V, with scan speeds in the range from 5 to 200 mV s^{-1}. Figure 9a–c presents the CV profiles of the symmetrical coin cells for supercapacitors based on the three 3D Try-CMPs, measured at the various scan rates. The practically rectangular forms of these CV curves resulted from the combined EDLC and pseudocapacitive behavior of the electrode materials.[37,40,68−70] The current density increased upon increasing the scan speed, demonstrating the high stability and rapid kinetics of these electrode materials.[37,40,68−70] Figure 9d–f displays the GCD curves of all three 3D Try-CMPs, tested at various current densities in the range from 0.5 to 10 A g^{-1}. These GCD curves were triangular with a small bend, suggesting both pseudocapacitive and EDLC properties.[37,40] The discharge times from such curves can usually be correlated to the specific capacitance.[37,40] Accordingly, the GCD curves of these CMPs suggested that the Try-Ph-TPE CMP took the longest time to discharge, an indication of its higher capacitance, followed by the Try-Ph-Th CMP and then the Try-Ph-Py CMP [Figure 9f]. The specific capacities of the Try-Ph-Th, Try-Ph-Py, and Try-Ph-TPE CMPs at 0.5 A g^{-1} were 53, 84.2, and 166 F g^{-1}, respectively [Figure 10a]. This behavior could also be related to the surface areas of these porous materials. Figure 10b displays the long-term cycling stability evaluated by measuring the

https://doi.org/10.1021/acsaem.2c02809
ACS Appl. Energy Mater. XXXX, XXX, XXX−XXX

charge/discharge process over 5000 cycles at a relatively high current density of 5 A g^{-1}. Here, all three of these porous polymers employed as electrode materials for symmetric supercapacitor coin cells displayed outstanding capacity retention: 91.0, 92.0, and 97.0% for the Try-Ph-Th, Try-Ph-Py, and Try-Ph-TPE CMPs, respectively. As displayed in Figure 10b, the coin cell incorporating the Try-Ph-TPE CMP delivered the highest percentage capacity retention (>97%). Furthermore, the calculated energy densities for the Try-Ph-Th, Try-Ph-Py, and Try-Ph-TPE CMPs were 7.3, 11.7, and 23.1 W h kg^{-1}, respectively (Figure S30). We revealed that 3D Try-CMP SSC devices showed high energy density values compared with other reported SSC devices [Table S2]. SEM images at different magnifications revealed that the Try-Ph-TPE CMP had small agglomerated spherical particles after electrochemical experiments, as presented in Figure S31. Figure S32 reveals that the Try-Ph-TPE CMP could power a glowing LED. Thus, the outstanding performance of these coin cell supercapacitors reveals the potential capability of such porous compounds for real and hybrid electric energy storage applications.

CONCLUSIONS

We used Suzuki cross-coupling to prepare three novel 3D Try-CMPs containing Try moieties. TGA revealed that both the Try-Ph-Py and Try-Ph-TPE CMPs had high values of T_{d10} (605 and 517 °C, respectively) with a char yield of up to 70 wt%. In addition, the Try-Ph-TPE CMP possessed a high specific surface area (715 m^2 g^{-1}) and pore volume (0.45 cm^3 g^{-1}). We evaluated the electrochemical performance of both three-electrode systems and symmetrical supercapacitor coin cells based on these three CMPs, with an eye on real applications. In the three-electrode and coin cell supercapacitors, the Try-Ph-TPE CMP delivered outstanding specific capacities of 245 and 166 F g^{-1}, respectively, at a current density of 0.5 A g^{-1}, superior to those of the other porous polymers used as electrode materials. In addition, the Try-Ph-TPE CMP exhibited superior cycling stability over 2000 charge/discharge cycles at a relatively high current density of 10 A g^{-1}; the capacity retentions were greater than 93.0% for the three-electrode system and 97.0% for the supercapacitor coin cell after 5000 cycles of charging/discharging at a current density of 5 A g^{-1}. Thus, because of their good specific capacitances, facile synthesis, high surface areas, and tunable morphologies, our new Try-linked CMPs appear to be excellent candidate materials for use in energy storage.

ASSOCIATED CONTENT

Supporting Information

The Supporting Information is available free of charge at https://pubs.acs.org/doi/10.1021/acsaem.2c02809.

Details about characterization methods and electrochemical analysis, summary of the specific capacitances of Try-Ph-Th, Try-Ph-Py, and Try-Ph-TPE CMPs compared to other porous materials, schematic scheme for all synthesized monomers and their spectroscopic and thermal stability analyses, XRD, SEM-EDS, TEM-EDX, XPS data, and Ragone plot of the as-prepared Try-Ph-Th, Try-Ph-Py, and Try-Ph-TPE CMPs, and the glowing LED photograph with a Try-Ph-TPE CMP symmetric coin supercapacitor (PDF)

AUTHOR INFORMATION

Corresponding Authors

Mohamed Gamal Mohamed − *Department of Materials and Optoelectronic Science, College of Semiconductor and Advanced Technology Research, Center for Functional Polymers and Supramolecular Materials, National Sun Yat-sen University, Kaohsiung 804, Taiwan; Chemistry Department, Faculty of Science, Assiut University, Assiut 71515, Egypt;* orcid.org/0000-0003-0301-8372; Email: mgamal.eldin12@yahoo.com

Shiao-Wei Kuo − *Department of Materials and Optoelectronic Science, College of Semiconductor and Advanced Technology Research, Center for Functional Polymers and Supramolecular Materials, National Sun Yat-sen University, Kaohsiung 804, Taiwan; Department of Medicinal and Applied Chemistry, Kaohsiung Medical University, Kaohsiung 807, Taiwan;* orcid.org/0000-0002-4306-7171; Email: kuosw@faculty.nsysu.edu.tw

Authors

Tzu-Hsin Weng − *Department of Materials and Optoelectronic Science, College of Semiconductor and Advanced Technology Research, Center for Functional Polymers and Supramolecular Materials, National Sun Yat-sen University, Kaohsiung 804, Taiwan*

Santosh U Sharma − *International PhD Program for Science and Department of Chemistry, National Sun Yat-sen University, Kaohsiung 80424, Taiwan*

Swetha V Chaganti − *International PhD Program for Science and Department of Chemistry, National Sun Yat-sen University, Kaohsiung 80424, Taiwan*

Maha Mohamed Samy − *Department of Materials and Optoelectronic Science, College of Semiconductor and Advanced Technology Research, Center for Functional Polymers and Supramolecular Materials, National Sun Yat-sen University, Kaohsiung 804, Taiwan; Chemistry Department, Faculty of Science, Assiut University, Assiut 71515, Egypt*

Jyh-Tsung Lee − *International PhD Program for Science, National Sun Yat-sen University, Kaohsiung 80424, Taiwan; Department of Medicinal and Applied Chemistry, Kaohsiung Medical University, Kaohsiung 807, Taiwan;* orcid.org/0000-0002-2658-4222

Complete contact information is available at: https://pubs.acs.org/10.1021/acsaem.2c02809

Notes

The authors declare no competing financial interest.

ACKNOWLEDGMENTS

This study was supported financially by the Ministry of Science and Technology, Taiwan, under contracts NSTC 110-2124-M-002-013 and 111-2223-E-110-004. The authors thank the staff at National Sun Yat-sen University for their assistance with the TEM (ID: EM022600) experiments.

REFERENCES

(1) Li, X. C.; Zhang, Y.; Wang, C. Y.; Wan, Y.; Lai, W. Y.; Pang, H.; Huang, W. Redox-Active Triazatruxene-Based Conjugated Microporous Polymers for High-Performance Supercapacitors. *Chem. Sci.* **2017**, *8*, 2959−2965.

(2) Najib, S.; Erdem, E. Current progress achieved in novel materials for supercapacitor electrodes: mini review. *Nanoscale Adv.* **2019**, *1*, 2817−2827.

(3) Samy, M. M.; Mohamed, M. G.; El-Mahdy, A. F. M.; Mansoure, T. H.; Wu, K. C. W.; Kuo, S. W. High-Performance Supercapacitor Electrodes Prepared From Dispersions of Tetrabenzonaphthalene-Based Conjugated Microporous Polymers and Carbon Nanotubes. *ACS Appl. Mater. Interfaces* **2021**, *13*, 51906−51916.
(4) Lyu, W.; Yan, C.; Chen, Z.; Chen, J.; Zuo, H.; Teng, L.; Liu, H.; Wang, L.; Liao, Y. Spirobifluorene-Based Conjugated Microporous Polymer-Grafted Carbon Nanotubes for Efficient Supercapacitive Energy Storage. *ACS Appl. Energy Mater.* **2022**, *5*, 3706−3714.
(5) Samy, M. M.; Mohamed, M. G.; Kuo, S. W. Pyrene-functionalized tetraphenylethylene polybenzoxazine for dispersing single-walled carbon nanotubes and energy storage. *Compos. Sci. Technol.* **2020**, *199*, No. 108360.
(6) Mohamed, M. G.; Mansoure, T. H.; Takashi, Y.; Samy, M. M.; Chen, T.; Kuo, S.-W. Ultrastable porous organic/inorganic polymers based on polyhedral oligomeric silsesquioxane (POSS) hybrids exhibiting high performance for thermal property and energy storage. *Microporous Mesoporous Mater.* **2021**, *328*, No. 111505.
(7) Mohamed, M. G.; EL-Mahdy, A. F. M.; Meng, T.-S.; Samy, M. M.; Kuo, S.-W. Multifunctional Hypercrosslinked Porous Organic Polymers Based on Tetraphenylethene and Triphenylamine Derivatives for High-Performance Dye Adsorption and Supercapacitor. *Polymers* **2020**, *12*, 2426.
(8) Wulan Septiani, N. L.; Kaneti, Y. V.; Fathoni, K. B.; Wang, J.; Ide, Y.; Yuliarto, B.; Nugraha; Dipojono, H. K.; Nanjundan, A. K.; Golberg, D.; Bando, Y.; Yamauchi, Y. Self-Assembly of Nickel Phosphate-Based Nanotubes into Two-Dimensional Crumpled Sheet-Like Architectures for High-Performance Asymmetric Supercapacitors. *Nano Energy* **2020**, *67*, No. 104270.
(9) Wang, Q.; Zhu, M.; Chen, G.; Dudko, N.; Li, Y.; Liu, H.; Shi, L.; Wu, G.; Zhang, D. High-Performance Microsized Si Anodes for Lithium-Ion Batteries: Insights into the Polymer Configuration Conversion Mechanism. *Adv. Mater.* **2022**, *34*, 2109658.
(10) Liu, S.; Kang, L.; Henzie, J.; Zhang, J.; Ha, J.; Amin, M. A.; Hossain, M. S. A.; Jun, S. C.; Yamauchi, Y. Recent Advances and Perspectives of Battery-Type Anode Materials for Potassium Ion Storage. *ACS Nano* **2021**, *15*, 18931−18973.
(11) Kim, D.; Kang, J.; Yan, B.; Seong, K.-d.; Piao, Y. Ambient Temperature Synthesis of Iron-Doped Porous Nickel Pyrophosphate Nanoparticles with Long-Term Chemical Stability for High-Performance Oxygen Evolution Reaction Catalysis and Supercapacitors. *ACS Sustainable Chem. Eng.* **2020**, *8*, 2843−2853.
(12) Li, L.; Lu, F.; Xue, R.; Ma, B.; Li, Q.; Wu, N.; Liu, H.; Yao, W.; Guo, H.; Yang, W. Ultrastable triazine-based covalent organic framework with an interlayer hydrogen bonding for supercapacitor applications. *ACS Appl. Mater. Interfaces* **2019**, *11*, 26355−26363.
(13) Young, C.; Park, T.; Yi, J. W.; Kim, J.; Hossain, M. S. A.; Kaneti, Y. V.; Yamauchi, Y. Advanced Functional Carbons and Their Hybrid Nanoarchitectures Towards Supercapacitor Applications. *ChemSusChem* **2018**, *11*, 3546−3558.
(14) Xu, Z.; Sun, S.; Han, Y.; Wei, Z.; Cheng, Y.; Yin, S.; Cui, W. High-Energy-Density Asymmetric Supercapacitor Based on a Durable and Stable Manganese Molybdate Nanostructure Electrode for Energy Storage Systems. *ACS Appl. Energy Mater.* **2020**, *3*, 5393−5404.
(15) Khattak, A. M.; Sin, H.; Ghazi, Z. A.; He, X.; Liang, B.; Khan, N. A.; Alanagh, H. R.; Iqbal, A.; Li, L.; Tang, Z. Controllable fabrication of redox-active conjugated microporous polymer on reduced graphene oxide for high performance faradaic energy storage. *J. Mater. Chem. A* **2018**, *6*, 18827−18832.
(16) Mei, L.; Wei, J.-C.; Duan, Q. Construction of copper porphyrinlinked conjugated microporous polymer/carbon nanotube composite as flexible electrodes for supercapacitors. *J. Mater. Sci.: Mater. Electron.* **2021**, *32*, 24953−24963.
(17) Amin, K.; Ashraf, N.; Mao, L.; Faul, C. F. J.; Wei, Z. Conjugated microporous polymers for energy storage: Recent progress and challenges. *Nano Energy* **2021**, *85*, No. 105958.
(18) Mohamed, M. G.; Ahmed, M. M. M.; Du, W.-T.; Kuo, S.-W. Meso/Microporous Carbons from Conjugated Hyper-Crosslinked Polymers Based on Tetraphenylethene for High-Performance CO_2 Capture and Supercapacitor. *Molecules* **2021**, *26*, 738.
(19) Mohamed, M. G.; Chaganti, S. V.; Sharma, S. U.; Samy, M. M.; Ejaz, M.; Lee, J. T.; Zhang, K.; Kuo, S. W. Constructing Conjugated Microporous Polymers Containing the Pyrene-4,5,9,10-Tetraone Unit for Energy Storage. *ACS Appl. Energy Mater.* **2022**, *5*, 10130−10140.
(20) Elewa, A. M.; EL-Mahdy, A. F. M.; Elsayed, M. H.; Mohamed, M. G.; Kuo, S. W.; Chou, H. H. Sulfur-doped triazine-conjugated microporous polymers for achieving the robust visible-light-driven hydrogen evolution. *Chem. Eng. J.* **2021**, *421*, No. 129825.
(21) Zheng, S.; Miao, L.; Sun, T.; Li, L.; Ma, T.; Bao, J.; Tao, Z.; Chen, J. An extended carbonyl-rich conjugated polymer cathode for high-capacity lithium-ion batteries. *J. Mater. Chem. A* **2021**, *9*, 2700−2705.
(22) Mohamed, M. G.; Elsayed, M. H.; Elewa, A. M.; EL-Mahdy, A. F. M.; Yang, C. H.; Mohammed, A. A. K.; Chou, H. H.; Kuo, S. W. Pyrene-containing conjugated organic microporous polymers for photocatalytic hydrogen evolution from water. *Catal. Sci. Technol.* **2021**, *11*, 2229−2241.
(23) Tan, Z.; Su, H.; Guo, Y.; Liu, H.; Liao, B.; Amin, A. M.; Liu, Q. Ferrocene-Based Conjugated Microporous Polymers Derived from Yamamoto Coupling for Gas Storage and Dye Removal. *Polymers* **2020**, *12*, 719.
(24) Lou, X.; Chen, J.; Xiong, Z.; Tang, D.; Chen, X.; Chen, S.; Dong, R.; Ye, C.; Qiu, T. Porosity Design on Conjugated Microporous Poly(Aniline)S for Exceptional Mercury(II) Removal. *ACS Appl. Mater. Interfaces* **2021**, *13*, 61653−61660.
(25) Mohamed, M. G.; Tsai, M.-Y.; Wang, C.-F.; Huang, C.-F.; Danko, M.; Dai, L.; Chen, T.; Kuo, S.-W. Multifunctional Polyhedral Oligomeric Silsesquioxane (POSS) Based Hybrid Porous Materials for CO_2 Uptake and Iodine Adsorption. *Polymers* **2021**, *13*, 221.
(26) Liu, S.; Kang, L.; Zhang, J.; Jung, E.; Lee, S.; Jun, S. C. Structural engineering and surface modification of MOF-derived cobalt-based hybrid nanosheets for flexible solid-state supercapacitors. *Energy Storage Mater.* **2020**, *32*, 167−177.
(27) Abuzeid, H. R.; EL-Mahdy, A. F. M.; Kuo, S. W. Covalent organic frameworks: Design principles, synthetic strategies, and diverse applications. *Giant* **2021**, *6*, No. 100054.
(28) Roh, D. H.; Shin, H.; Kim, H. T.; Kwon, T. H. Sono-Cavitation and Nebulization-Based Synthesis of Conjugated Microporous Polymers for Energy Storage Applications. *ACS Appl. Mater. Interfaces* **2021**, *13*, 61598−61609.
(29) Wang, H.; Cheng, Z.; Liao, Y.; Li, J.; Weber, J.; Thomas, A.; Faul, C. F. J. Conjugated Microporous Polycarbazole Networks as Precursors for Nitrogen-Enriched Microporous Carbons for CO_2 Storage and Electrochemical Capacitors. *Chem. Mater.* **2017**, *29*, 4885−4893.
(30) Mohamed, M. G.; Chaganti, S. V.; Li, M. S.; Samy, M. M.; Sharma, S. U.; Lee, J. T.; Elsayed, M. H.; Chou, H. H.; Kuo, S. W. Ultrastable Porous Organic Polymers Containing Thianthrene and Pyrene Units as Organic Electrode Materials for Supercapacitors. *ACS Appl. Energy Mater.* **2022**, *5*, 6442−6452.
(31) Mohamed, M. G.; Sharma, S. U.; Yang, C.-H.; Samy, M. M.; Mohammed, A. A. K.; Chaganti, S. V.; Lee, J.-T.; Wei-Kuo, S. Anthraquinone-Enriched Conjugated Microporous Polymers as Organic Cathode Materials for High-Performance Lithium-Ion Batteries. *ACS Appl. Energy Mater.* **2021**, *4*, 14628−14639.
(32) Jiang, X.; Zhang, K.; Huang, Y.; Xu, B.; Xu, X.; Zhang, J.; Liu, Z.; Wang, Y.; Pan, Y.; Bian, S.; Chen, Q.; Wu, X.; Zhang, G. Conjugated Microporous Polymer with C≡C and C−F Bonds: Achieving Remarkable Stability and Super Anhydrous Proton Conductivity. *ACS Appl. Mater. Interfaces* **2021**, *13*, 15536−15541.
(33) Weng, Z.; Su, Y.; Wang, D. W.; Li, F.; Du, J.; Cheng, H. M. Graphene−cellulose paper flexible supercapacitors. *Adv. Energy Mater.* **2011**, *1*, 917−922.
(34) Liu, Z.; Yin, Y.; Eginligil, M.; Wang, L.; Liu, J.; Huang, W. Two-dimensional conjugated microporous polymer films: fabrication strategies and potential applications. *Polym. Chem.* **2021**, *12*, 807−821.
(35) Lee, J.-S. M.; Cooper, A. I. Advances in conjugated microporous polymers. *Chem. Rev.* **2020**, *120*, 2171−2214.

https://doi.org/10.1021/acsaem.2c02809
ACS Appl. Energy Mater. XXXX, XXX, XXX−XXX

(36) Lee, J.-S. M.; Wu, T.-H.; Alston, B. M.; Briggs, M. E.; Hasell, T.; Hu, C.-C.; Cooper, A. I. Porosity-engineered carbons for supercapacitive energy storage using conjugated microporous polymer precursors. *J. Mater. Chem. A* **2016**, *4*, 7665−7673.
(37) Mohamed, M. G.; Sharma, S. U.; Liu, N. Y.; Mansoure, T. H.; Samy, M. M.; Chaganti, S. V.; Chang, Y. L.; Lee, J. T.; Kuo, S. W. Ultrastable Covalent Triazine Organic Framework Based on Anthracene Moiety as Platform for High-Performance Carbon Dioxide Adsorption and Supercapacitors. *Int. J. Mol. Sci.* **2022**, *23*, 3174.
(38) Samy, M. M.; Sharma, S. U.; Mohamed, M. G.; Mohammed, A. A. K.; Chaganti, S. V.; Lee, J. T.; Kuo, S. W. Conjugated microporous polymers containing ferrocene units for high carbon dioxide uptake and energy storage. *Mater. Chem. Phys.* **2022**, *287*, No. 126177.
(39) Mohamed, M. G.; Chen, T. C.; Kuo, S. W. Solid-State Chemical Transformations to Enhance Gas Capture in Benzoxazine-Linked Conjugated Microporous Polymers. *Macromolecules* **2021**, *54*, 5866−5877.
(40) EL-Mahdy, A. F. M.; Yu, T. C.; Mohamed, M. G.; Kuo, S. W. Secondary Structures of Polypeptide-Based Diblock Copolymers Influence the Microphase Separation of Templates for the Fabrication of Microporous Carbons. *Macromolecules* **2021**, *54*, 1030−1042.
(41) Das, S.; Heasman, P.; Ben, T.; Qiu, S. Porous organic materials: strategic design and structure−function correlation. *Chem. Rev.* **2017**, *117*, 1515−1563.
(42) Samy, M. M.; Mohamed, M. G.; Mansoure, T. H.; Meng, T. S.; Khan, M. A. R.; Liaw, C. C.; Kuo, S. W. Solid state chemical transformations through ring-opening polymerization of ferrocene-based conjugated microporous polymers in host−guest complexes with benzoxazine-linked cyclodextrin. *J. Taiwan Inst. Chem. Eng.* **2022**, *132*, 104110.
(43) Mohamed, M. G.; EL-Mahdy, A. F. M.; Kotp, M. G.; Kuo, S. W. Advances in porous organic polymers: syntheses, structures, and diverse applications. *Mater. Adv.* **2022**, *3*, 707−733.
(44) Liao, Y.; Wang, H.; Zhu, M.; Thomas, A. Efficient Supercapacitor Energy Storage Using Conjugated Microporous Polymer Networks Synthesized from Buchwald−Hartwig Coupling. *Adv. Mater.* **2018**, *30*, 1705710.
(45) Mohamed, M. G.; Samy, M. M.; Mansoure, T. H.; Sharma, S. U.; Tsai, M. S.; Chen, J. H.; Lee, J. T.; Kuo, S. W. Dispersions of 1,3,4-Oxadiazole-Linked Conjugated Microporous Polymers with Carbon Nanotubes as a High-Performance Electrode for Supercapacitors. *ACS Appl. Energy Mater.* **2022**, *5*, 3677−3688.
(46) Samy, M. M.; Mekhemer, I. M. A.; Mohamed, M. G.; Elsayed, M. H.; Lin, K.-H.; Chen, Y.-K.; Wu, T.-L.; Chou, H.-H.; Kuo, S.-W. Conjugated microporous polymers incorporating Thiazolo[5,4-d]-thiazole moieties for Sunlight-Driven hydrogen production from water. *Chem. Eng. J.* **2022**, *446*, No. 137158.
(47) Lin, Z.; Goikolea, E.; Balducci, A.; Naoi, K.; Taberna, P. L.; Salanne, M.; Yushin, G.; Simon, P. Materials for Supercapacitors: When Li-Ion Battery Power is not Enough. *Mater. Today* **2018**, *21*, 419−436.
(48) Mohamed, M. G.; Mansoure, T. H.; Samy, M. M.; Takashi, Y.; Mohammed, A. A. K.; Ahamad, T.; Alshehri, S. M.; Kim, J.; Matsagar, B. M.; Wu, K. C. W.; Kuo, S. W. Ultrastable Conjugated Microporous Polymers Containing Benzobisthiadiazole and Pyrene Building Blocks for Energy Storage Applications. *Molecules* **2022**, *27*, 2025.
(49) Wang, Y.; Song, Y.; Xia, Y. Electrochemical capacitors: mechanism, materials, systems, characterization and applications. *Chem. Soc. Rev.* **2016**, *45*, 5925−5950.
(50) Mohamed, M. G.; Atayde, E. C., Jr.; Matsagar, M. B.; Na, J.; Yamauchi, Y.; Wu, K. C. W.; Kuo, S. W. Construction Hierarchically Mesoporous/Microporous Materials Based on Block Copolymer and Covalent Organic Framework. *J. Taiwan Inst. Chem. Eng.* **2020**, *112*, 180−192.
(51) Mohamed, M. G.; Samy, M. M.; Mansoure, T. H.; Li, C. J.; Li, W. C.; Chen, J. H.; Zhang, K.; Kuo, S. W. Microporous Carbon and Carbon/Metal Composite Materials Derived from Bio-Benzoxazine-Linked Precursor for CO_2 Capture and Energy Storage Applications. *Int. J. Mol. Sci.* **2022**, *23*, 347.
(52) Zhou, Z.; Li, X.; Guo, D.; Shinde, D. B.; Lu, D.; Chen, L.; Liu, X.; Cao, L.; Aboalsaud, A. M.; Hu, Y.; Lai, Z. Electropolymerization of robust conjugated microporous polymer membranes for rapid solvent transport and narrow molecular sieving. *Nat. Commun.* **2020**, *11*, 5323.
(53) Yu, K.; Pan, X.; Zhang, G.; Liao, X.; Zhou, X.; Yan, M.; Xu, L.; Mai, L. Nanowires in Energy Storage Devices: Structures, Synthesis, and Applications. *Adv. Energy Mater.* **2018**, *8*, 1802369.
(54) Chen, D.; Jiang, K.; Huang, T.; Shen, G. Recent Advances in Fiber Supercapacitors: Materials, Device Configurations, and Applications. *Adv. Mater.* **2020**, *32*, 1901806.
(55) Mothika, V. S.; Baumgarten, M.; Scherf, U. Neutral, π-Radical-Conjugated Microporous Polymer Films of Nanoscale Thickness for Potential Use in Magnetoelectronics and Sensor Devices. *ACS Appl. Nano Mater.* **2019**, *2*, 4832−4841.
(56) Pallavi, P.; Bandyopadhyay, S.; Louis, J.; Deshmukh, A.; Patra, A. A Soluble Conjugated Porous Organic Polymer: Efficient White Light Emission in Solution, Nanoparticles, Gel and Transparent Thin Film. *Chem. Commun.* **2017**, *53*, 1257−1260.
(57) Woźny, M.; Mames, A.; Ratajczyk, T. Triptycene Derivatives: From Their Synthesis to Their Unique Properties. *Molecules* **2022**, *27*, 250.
(58) Bartlett, P. D.; Ryan, M. J.; Cohen, S. G. Triptycene1 (9,10-O-Benzenoanthracene). *J. Am. Chem. Soc.* **1942**, *64*, 2649−2653.
(59) Jiang, Y.; Chen, C. F. Recent Developments in Synthesis and Applications of Triptycene and Pentiptycene Derivatives. *Eur. J. Org. Chem.* **2011**, *2011*, 6377−6403.
(60) Reinhard, D.; Zhang, W. S.; Vaynzof, Y.; Rominger, F.; Schröder, R. R.; Mastalerz, M. Triptycene-based porous metal-assisted salphen organic frameworks: influence of the metal ions on formation and gas sorption. *Chem. Mater.* **2018**, *30*, 2781−2790.
(61) Hassan, A.; Alam, A.; Ansari, M.; Das, N. Hydroxy functionalized triptycene based covalent organic polymers for ultra-high radioactive iodine uptake. *Chem. Eng. J.* **2022**, *427*, No. 130950.
(62) Peurifoy, S. R.; Russell, J. C.; Sisto, T. J.; Yang, Y.; Roy, X.; Nuckolls, C. Designing three-dimensional architectures for high-performance electron accepting pseudocapacitors. *J. Am. Chem. Soc.* **2018**, *140*, 10960−10964.
(63) Zhang, C.; Zhu, P. C.; Tan, L.; Luo, L. N.; Liu, Y.; Liu, J. M.; Ding, S. Y.; Tan, B.; Yang, X. L.; Xu, H. B. Synthesis and properties of organic microporous polymers from the monomer of hexaphenylbenzene based triptycene. *Polymer* **2016**, *82*, 100−104.
(64) Ejaz, M.; Mohamed, M. G.; Sharma, S. U.; Lee, J. T.; Huang, C. F.; Chen, T.; Kuo, S. W. An Ultrastable Porous Polyhedral Oligomeric Silsesquioxane/Tetraphenylthiophene Hybrid as a High-Performance Electrode for Supercapacitors. *Molecules* **2022**, *27*, 6238.
(65) Rafik, F.; Gualous, H.; Gallay, R.; Crausaz, A.; Berthon, A. Frequency, thermal and voltage supercapacitor characterization and modeling. *J. Power Sources* **2007**, *165*, 928−934.
(66) Samy, M. M.; Mohamed, M. G.; Kuo, S. W. Directly synthesized nitrogen-and-oxygen−doped microporous carbons derived from a bio-derived polybenzoxazine exhibiting high-performance supercapacitance and CO_2 uptake. *Eur. Polym. J.* **2020**, *138*, No. 109954.
(67) Mohamed, M. G.; Hu, H.-Y.; Madhu, M.; Ejaz, M.; Sharma, S. U.; Tseng, W.-L.; Samy, M. M.; Huang, C.-W.; Lee, J.-T.; Kuo, S.-W. Construction of Ultrastable Conjugated Microporous Polymers Containing Thiophene and Fluorene for Metal Ion Sensing and Energy Storage. *Micromachines* **2022**, *13*, 1466.
(68) Li, Y.; Zheng, S.; Liu, X.; Li, P.; Sun, L.; Yang, R.; Wang, S.; Wu, Z. S.; Bao, X.; Deng, W. Q. Conductive microporous covalent triazine-based framework for high-performance electrochemical capacitive energy storage. *Angew. Chem., Int. Ed.* **2018**, *130*, 8124−8128.
(69) Hu, F.; Wang, J.; Hu, S.; Li, L.; Shao, W.; Qiu, J.; Lei, Z.; Deng, W.; Jian, X. Engineered fabrication of hierarchical frameworks with tuned pore structure and N, O-co-doping for high-performance supercapacitors. *ACS Appl. Mater. Interfaces* **2017**, *37*, 31940−31949.
(70) Khattak, A. M.; Ghazi, Z. A.; Liang, B.; Khan, N. A.; Iqbal, A.; Li, L.; Tang, Z. A redox-active 2D covalent organic framework with pyridine moieties capable of faradaic energy storage. *J. Mater. Chem. A* **2016**, *4*, 16312−16317.

https://doi.org/10.1021/acsaem.2c02809
ACS Appl. Energy Mater. XXXX, XXX, XXX−XXX